Implementation of a piecewise Drucker-Prager model in Abaqus

Kwangmin Lee [*], Karuppasamy Pandian Marimuthu [*], Hyungyil Lee [*]

* Department of Mechanical Engineering, Sogang University, Seoul 04107, Rep. of Korea

***Abstract**: Due to size effect in nanotechnology, an appropriate pressure-dependent model is required to define the material yielding in ceramics. Current pressure-dependent models, such as the Mohr-Coulomb and Drucker-Prager (DP) models, have specific shapes and thus cannot be flexibly applied to ceramic materials. This study develops a constitutive model, an integration algorithm, and consistent tangent operators for a piecewise Drucker-Prager (PDP) model. The constitutive model with considering strain hardening with yield flows is derived. The integration algorithm is developed based on return mapping (to smooth portion, apex and corner). The consistent tangent operators are established for each return mapping case. The PDP model is then implemented in commercial finite element code (using Abaqus) by developing a user material subroutine (UMAT). This UMAT is verified for bilinear and extended DP models through finite element analysis (FEA) of a hydrostatic test with a single element. We expect that the UMAT for the PDP model can be used to describe the plastic behavior of pressure-dependent materials accurately.*

***Keywords**: Piecewise Drucker-Prager yield model, Numerical implementation, Constitutive modeling, UMAT, FEM.*

1. Introduction

The classical Drucker-Prager (DP) model is a pressure-dependent yield model in which yield strength and hydrostatic pressure are linearly related (Drucker and Prager, 1952). In addition to the linear DP model, extended DP models also have hyperbolic and general exponent forms (Abaqus, 2013). However, since existing models have a limitation that cannot be modified to fit the yielding model of any material, a piecewise Drucker-Prager (PDP) criterion is required. Most commercial finite element analysis (FEA) programs do not have a built-in PDP model, although a simple PDP model where strain hardening is not implemented is available in the commercial finite element software, Autodyn (Ansys, 2015). To establish and popularize a user subroutine for an enhanced PDP model, more careful and detailed research about constitutive equations, integration algorithm and consistent tangent operators of the PDP model is required.

The present study develops an elasto-plastic constitutive model, an integration algorithm based on return mapping, and consistent tangent operators for PDP model in which strain hardening can be considered. The return mapping method and tangent operators are developed at the intersection where piecewise linear DP models meet. Based on the developed constitutive model and numerical implementation techniques, a user material subroutine (UMAT) for the PDP model is developed and then verified by using single element triaxial finite element (FE) simulations.

2. Piecewise Drucker-Prager model

In some materials, an extended pressure-dependent model is needed to describe material's plastic behavior (Ma *et al*., 1998; Milani and Lourenco, 2009). However, since it is difficult to directly make a UMAT for the extended pressure-dependent model by using its constitutive equations due to the complexity of update formula, we develop PDP model by combining several linear DP models to describe extended DP model.

2.1 Piecewise Drucker-Prager (PDP) constitutive model

In a PDP model (Fig. 1), multiple linear DP models are combined.

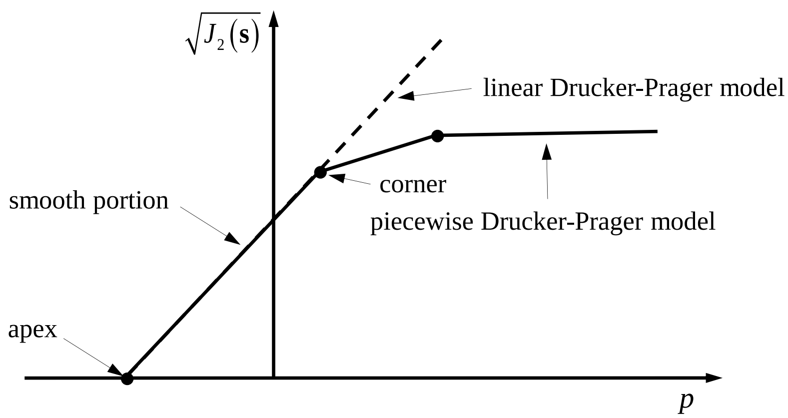

Fig. 1 Schematic comparison of linear and piecewise Drucker-Prager models

The yield function of the PDP model is defined by

$$\Phi^i(\boldsymbol{\sigma}, c_i) = \sqrt{J_2(\mathbf{s}(\boldsymbol{\sigma}))} + \eta_i\, p(\boldsymbol{\sigma}) - \xi_i c_i \qquad (i = 1, 2, \ldots, n) \tag{1}$$

Here

$$J_2 = \frac{1}{2}\mathbf{s}:\mathbf{s} \quad ; \quad \mathbf{s} = \boldsymbol{\sigma} - p(\boldsymbol{\sigma})\mathbf{I} \quad ; \quad \mathbf{I} = \begin{bmatrix}1 & 1 & 1 & 0 & 0 & 0\end{bmatrix}^{\mathrm{T}} \tag{2}$$

where $\mathbf{s}$ is the deviatoric stress, $\boldsymbol{\sigma}$ is the stress, p is the hydrostatic pressure and c_i is the cohesion of the material. The η_i and ξ_i are constants derived from approximation to the piecewise Mohr-Coulomb (PMC) yield model (Fig. 2). The formulas for the outer edges are

$$\eta_i = \frac{6\sin\phi_i}{\sqrt{3}\,(3-\sin\phi_i)}, \qquad \xi_i = \frac{6\cos\phi_i}{\sqrt{3}\,(3-\sin\phi_i)} \qquad (i = 1, 2, \ldots, n) \tag{3}$$

whereas the formulas for the inner edges are

$$\eta_i = \frac{6\sin\phi_i}{\sqrt{3}\,(3+\sin\phi_i)}, \qquad \xi_i = \frac{6\cos\phi_i}{\sqrt{3}\,(3+\sin\phi_i)} \qquad (i = 1, 2, \ldots, n) \tag{4}$$

where ϕ_i is friction angle in the PMC model.

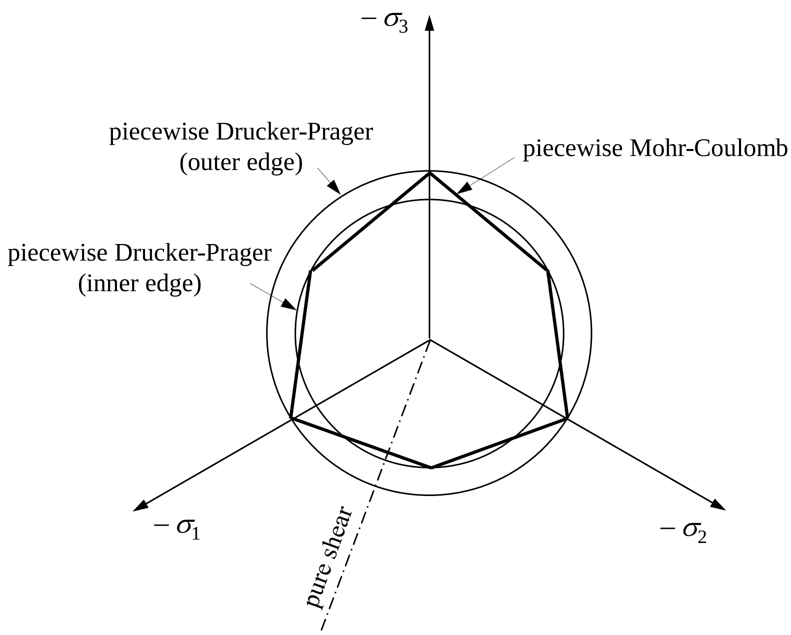

Fig. 2 π-plane section of piecewise Mohr-Coulomb surface and piecewise Drucker-Prager approximations

In the associative DP model, the yield function of Eq. (1) is employed as flow potential; correspondingly, three distinct plastic flows are described as follows.

(i) The plastic flow on the piecewise smooth portions of the yield surface is

$$\dot{\boldsymbol{\varepsilon}}^p = \dot{\gamma}\mathbf{N}^i \qquad (i = 1, 2, \ldots, n) \tag{5}$$

where $\dot{\boldsymbol{\varepsilon}}^p$ is plastic strain rate, $\dot{\gamma}$ is the plastic multiplier and $\mathbf{N}$ is the flow vector. The flow vector is

$$\mathbf{N}^i = \frac{\partial \Psi_i}{\partial \boldsymbol{\sigma}} = \frac{1}{2\sqrt{J_2(\mathbf{s})}}\mathbf{s} + \frac{\bar{\eta}_i}{3}\mathbf{I} \qquad (i = 1, 2, \ldots, n) \tag{6}$$

(ii) At the corner where two linear DP models meet, the plastic flow is

$$\dot{\boldsymbol{\varepsilon}}^p = \dot{\gamma}^i \mathbf{N}^i + \dot{\gamma}^{i+1} \mathbf{N}^{i+1} \qquad (i = 1, 2, \ldots, n-1) \tag{7}$$

where $\mathbf{N}^i$ and $\mathbf{N}^{i+1}$ are the flow vector of the ith and i+1th linear DP model.

(iii) The plastic flow vector at the apex singularity is a sub-gradient of the first linear DP model flow potential Ψ_1. The effective plastic strain rate, in this case, is (de Souza Neto *et al*., 2008)

$$\dot{\bar{\varepsilon}}^p = \dot{\gamma}\xi_1 \tag{8}$$

Since volumetric plastic strain rate $\dot{\varepsilon}_v^p$ is given as

$$\dot{\varepsilon}_v^p = \dot{\gamma}\bar{\eta}_1 \tag{9}$$

the effective plastic strain rate can thus be expressed as

$$\dot{\bar{\varepsilon}}^p = \frac{\xi_1}{\eta_1}\dot{\varepsilon}_v^p \tag{10}$$

To avoid excessive dilatancy, the non-associative flow rule is also used in the present PDP model as in the linear DP model. Since the PDP model is an approximation of the PMC model, the PDP yield function, as flow potential, is used with the dilatancy angle ψ_i instead of the friction angle ϕ_i ($\psi_i < \phi_i$); that is

$$\Psi_i(\boldsymbol{\sigma}, c_i) = \sqrt{J_2(\mathbf{s}(\boldsymbol{\sigma}))} + \bar{\eta}_i p \qquad (i = 1, 2, \ldots, n) \tag{11}$$

where $\bar{\eta}_i$ is obtained by replacing ϕ_i with ψ_i in the definition of η_i given by Eq. (3) or (4). In other words, if the outer cone approximation to the PMC criterion is applied, then

$$\bar{\eta}_i = \frac{6\sin\psi_i}{\sqrt{3}(3 - \sin\psi_i)} \qquad (i = 1, 2, \ldots, n) \tag{12}$$

while if the inner cone approximation is employed, then

$$\bar{\eta}_i = \frac{6\sin\psi_i}{\sqrt{3}\left(3+\sin\psi_i\right)} \qquad \left(i=1,2,\ldots,n\right) \tag{13}$$

In the non-associative DP model, by using Ψ_i and $\bar{\eta}_i$ instead of Φ_i and η_i in Eqs. (5)-(10), corresponding flow vectors can be obtained.

2.2 Integration algorithm for the PDP model

The general return-mapping update formula for the stress tensor of materials is

$$\boldsymbol{\sigma}_{n+1} = \boldsymbol{\sigma}_{n+1}^{\text{trial}} - \mathbf{D}^e : \Delta\boldsymbol{\varepsilon}^p \tag{14}$$

where $\mathbf{D}^e$ is an elasticity matrix. Since the flow vectors are different according to the location of the PDP model, three explicit forms exist for the return-mapping algorithm.

2.2.1 Return to the piecewise smooth portions

On the piecewise smooth portions, the flow vector is defined, as described in section 2.1. Then, plastic strain increment is

$$\Delta\boldsymbol{\varepsilon}^p = \Delta\gamma\,\mathbf{N}_{n+1}^i = \Delta\gamma\left(\frac{1}{2\sqrt{J_2(\mathbf{s})}}\mathbf{s}_{n+1} + \frac{\bar{\eta}_i}{3}\mathbf{I}\right) \qquad \left(i=1,2,\ldots,n\right) \tag{15}$$

The corresponding updated stress is

$$\begin{aligned}\boldsymbol{\sigma}_{n+1} &= \boldsymbol{\sigma}_{n+1}^{\text{trial}} - \Delta\gamma\left[2G\left(\mathbf{N}_d^i\right)_{n+1} + K\left(\mathbf{N}_v^i\right)_{n+1}\right] \\ &= \boldsymbol{\sigma}_{n+1}^{\text{trial}} - \Delta\gamma\left[\frac{G}{2\sqrt{J_2(\mathbf{s})}}\mathbf{s}_{n+1} + \frac{K\bar{\eta}_i}{3}\mathbf{I}\right] \qquad \left(i=1,2,\ldots,n\right)\end{aligned} \tag{16}$$

where G is the shear modulus, K is the bulk modulus, $\mathbf{N}_d$ is the deviatoric component of flow vector, and $\mathbf{N}_v$ is the volumetric flow vector. Eq. (16) can be simplified by noting that the following equality holds due to the definition of J_2

$$\frac{\mathbf{s}_{n+1}}{J_2\left(\mathbf{s}_{n+1}\right)} = \frac{\mathbf{s}_{n+1}^{\text{trial}}}{J_2\left(\mathbf{s}_{n+1}^{\text{trial}}\right)} \tag{17}$$

Then, substituting Eq. (17) into Eq. (16) provides the updated stress, expressed as

$$\boldsymbol{\sigma}_{n+1} = \boldsymbol{\sigma}_{n+1}^{\text{trial}} - \Delta\gamma \left[\frac{G}{2\sqrt{J_2\left(\mathbf{s}^{\text{trial}}\right)}} \mathbf{s}_{n+1}^{\text{trial}} + \frac{K\bar{\eta}_i}{3} \mathbf{I} \right] \qquad \left(i = 1, 2, \mathrm{K}, n\right) \tag{18}$$

The components of updated deviatoric stress s_{n+1} and hydrostatic stress p_{n+1} are then

$$\mathbf{s}_{n+1} = \left(1 - \frac{G\Delta\gamma}{\sqrt{J_2\left(\mathbf{s}_{n+1}^{\text{trial}}\right)}}\right) \mathbf{s}_{n+1}^{\text{trial}} \quad ; \quad p_{n+1} = p_{n+1}^{\text{trial}} - K\bar{\eta}_i \Delta\gamma \qquad \left(i = 1, 2, \mathrm{K}, n\right) \tag{19}$$

The consistency condition is

$$\Phi_{n+1}^{i} = \sqrt{J_2\left(\mathbf{s}_{n+1}\right)} + \eta_i\, p_{n+1} - \xi_i\, c_i\left(\bar{\varepsilon}_{n+1}^{p}\right) = 0 \qquad \left(i = 1, 2, \mathrm{K}, n\right) \tag{20}$$

Here the update effective plastic strain is

$$\bar{\varepsilon}_{n+1}^{p} = \bar{\varepsilon}_{n}^{p} + \Delta\bar{\varepsilon}^{P} \tag{21}$$

with

$$\Delta\bar{\varepsilon}^{P} = \xi\, \Delta\gamma \tag{22}$$

Applying Eq. (19) to the consistency condition yields the following equation for $\Delta\gamma$:

$$\tilde{\Phi}^{i}\left(\Delta\gamma\right) = \sqrt{J_2\left(\mathbf{s}_{n+1}^{\text{trial}}\right)} - G\Delta\gamma + \eta_i\left(p_{n+1}^{\text{trial}} - K\bar{\eta}_i\, \Delta\gamma\right) - \xi_i\, c_i\left(\bar{\varepsilon}_{n}^{p} + \xi_i\, \Delta\gamma\right) = 0 \qquad \left(i = 1, 2, \mathrm{K}, n\right) \tag{23}$$

By solving Eq. (23), the stress is updated by Eq. (19).

2.2.2 Return to the apex

At the apex, the consistency condition of Eq. (20) in the case of $i = 1$ is reduced to

$$c_1\left(\bar{\varepsilon}_{n}^{p} + \Delta\bar{\varepsilon}^{p}\right)\frac{\xi_1}{\bar{\eta}_1} - p_{n+1}^{\text{trial}} + K\Delta\varepsilon_{v}^{p} = 0 \tag{24}$$

Further, with the introduction of the discretized form of Eq. (10) for the non-associative DP model to Eq. (24), the final return-mapping equation for the DP apex can be obtained as

$$r\left(\Delta\varepsilon_{n}^{p}\right) = c_1\left(\bar{\varepsilon}_{n}^{p} + \alpha_1\Delta\bar{\varepsilon}^{p}\right)\beta - p_{n+1}^{\text{trial}} + K\Delta\varepsilon_{v}^{p} = 0 \tag{25}$$

where

$$\alpha_1 = \xi_1 / \eta_1, \qquad \beta = \xi_1 / \bar{\eta}_1 \tag{26}$$

This is geometrically shown in Fig. 3. After the solution of Eq. (25) is obtained for $\Delta\varepsilon_v^p$, the updated stress and effective plastic strain are obtained as

$$\begin{aligned} \bar{\varepsilon}_{n+1}^p &= \bar{\varepsilon}_n^p + \alpha_1 \Delta\varepsilon_v^p \\ \boldsymbol{\sigma}_{n+1} &= \left(p_{n+1}^{\text{trial}} - K\Delta\varepsilon_v^p \right) \mathbf{I} \end{aligned} \tag{27}$$

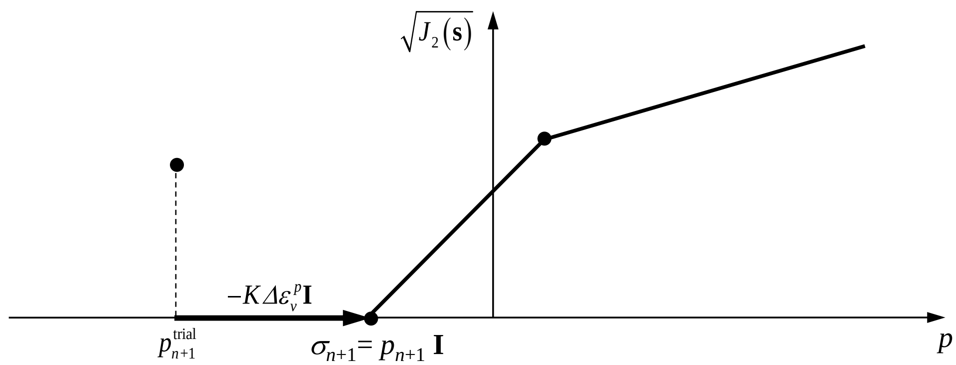

Fig. 3 Piecewise Drucker-Prager model; return mapping to apex

2.2.3 Return to the corner

A pressure at a corner, where the i^{th} and i+1$^{\text{th}}$ linear DP models are merged, is defined as critical pressure p_c. If $p > p_c$, the i^{th} linear DP model is applied, and if $p \leq p_c$, the i+1$^{\text{th}}$ linear DP model is applied to the material.

On return to the piecewise smooth portions, p_{n+1} is always smaller than p_{n+1}^{trial} by Eq. (19). Thus, in the PDP model, p_{n+1} can be smaller than p_c even when $p_{n+1}^{\text{trial}} > p_c$, which is inappropriate return mapping (Fig. 4a). To solve this problem, two plastic multipliers (γ^i and γ^{i+1}) for the i^{th} and i+1$^{\text{th}}$ linear DP models (which may be nonzero) are used. Then, the incremental plastic strain is

$$\Delta\varepsilon^p = \sum \Delta\gamma^i \mathbf{N}^i = \Delta\gamma^i \mathbf{N}^i + \Delta\gamma^{i+1} \mathbf{N}^{i+1} \tag{28}$$

where $\mathbf{N}^i$ and $\mathbf{N}^{i+1}$ are the normal vectors to the i^{th} and i+1$^{\text{th}}$ linear DP models, respectively. Recall that the general updated return-mapping formula for the stress tensor is

$$\boldsymbol{\sigma}_{n+1} = \boldsymbol{\sigma}_{n+1}^{\text{trial}} - \mathbf{D}^e : \Delta\boldsymbol{\varepsilon}^p \tag{29}$$

With Eq. (28), Eq. (29) is expressed as

$$\boldsymbol{\sigma}_{n+1} = \boldsymbol{\sigma}_{n+1}^{\mathrm{trial}} - \mathbf{D}^{e} : \sum \Delta\gamma^{i}\, \mathbf{N}_{n+1}^{i} \tag{30}$$

Then, the corresponding updated formula is

$$\boldsymbol{\sigma}_{n+1} = \boldsymbol{\sigma}_{n+1}^{\mathrm{trial}} - \sum \Delta\gamma^{i} \left[2G\left(\mathbf{N}_{d}^{i}\right)_{n+1} + K\left(\mathbf{N}_{v}^{i}\right)_{n+1} \right] \tag{31}$$

The components of updated deviatoric stress $\mathbf{s}_{n+1}$ and hydrostatic stress p_{n+1} are then

$$\begin{aligned} \mathbf{s}_{n+1} &= \left(1 - \frac{G\left(\Delta\gamma^{i} + \Delta\gamma^{i+1}\right)}{\sqrt{J\left(\mathbf{s}_{n+1}^{\mathrm{trial}}\right)}} \right) \mathbf{s}_{n+1}^{\mathrm{trial}} \\ p_{n+1} &= p_{n+1}^{\mathrm{trial}} - K\left(\bar{\eta}_{i}\,\Delta\gamma^{i} + \bar{\eta}_{i+1}\,\Delta\gamma^{i+1}\right) \end{aligned} \tag{32}$$

At the corner, the updated stresses are such that the equation of the i^{th} linear DP model, $\Phi^{i} = 0$, and the equation of the $i+1^{\mathrm{th}}$ linear DP model, $\Phi^{i+1} = 0$, are simultaneously fulfilled (Fig. 4b). These two equations have to be solved for $\Delta\gamma^{i}$ and $\Delta\gamma^{i+1}$

$$\begin{aligned} \Phi^{i}\left(\Delta\gamma^{i}, \Delta\gamma^{i+1}\right) &= \sqrt{J_{2}\left(\mathbf{s}_{n+1}^{\mathrm{trial}}\right)} - G\left(\Delta\gamma^{i} + \Delta\gamma^{i+1}\right) + \eta_{i}\left(p_{n+1}^{\mathrm{trial}} - K(\bar{\eta}_{i}\Delta\gamma^{i} + \bar{\eta}_{i+1}\Delta\gamma^{i+1})\right) \\ &\quad - \xi_{i}\, c_{i}\left(\bar{\varepsilon}_{n+1}^{p} + \Delta\bar{\varepsilon}^{p}\right) \\ \Phi^{i+1}\left(\Delta\gamma^{i}, \Delta\gamma^{i+1}\right) &= \sqrt{J_{2}\left(\mathbf{s}_{n+1}^{\mathrm{trial}}\right)} - G\left(\Delta\gamma^{i} + \Delta\gamma^{i+1}\right) + \eta_{i+1}\left(p_{n+1}^{\mathrm{trial}} - K(\bar{\eta}_{i}\Delta\gamma^{i} + \bar{\eta}_{i+1}\Delta\gamma^{i+1})\right) \\ &\quad - \xi_{i+1}\, c_{i+1}\left(\bar{\varepsilon}_{n+1}^{p} + \Delta\bar{\varepsilon}^{p}\right) \end{aligned} \tag{33}$$

Note that principle of this return mapping to the corner is similar to the modified DP/cap model, although when checking plastic admissibility in the PDP model, the pressure should also be considered with the yield function. This is because, in the modified DP/cap model, yield stress monotonically decreases after the corner (de Souza Neto *et al*., 2008), but in the PDP model, yield stress can increase.

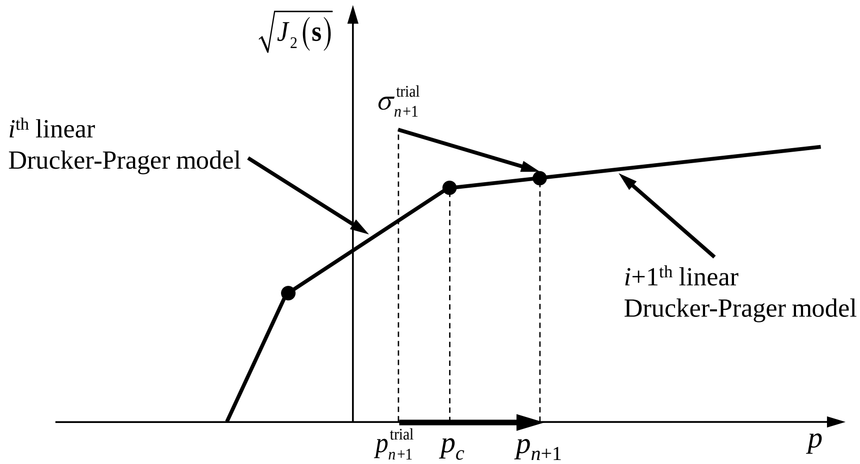

(a)

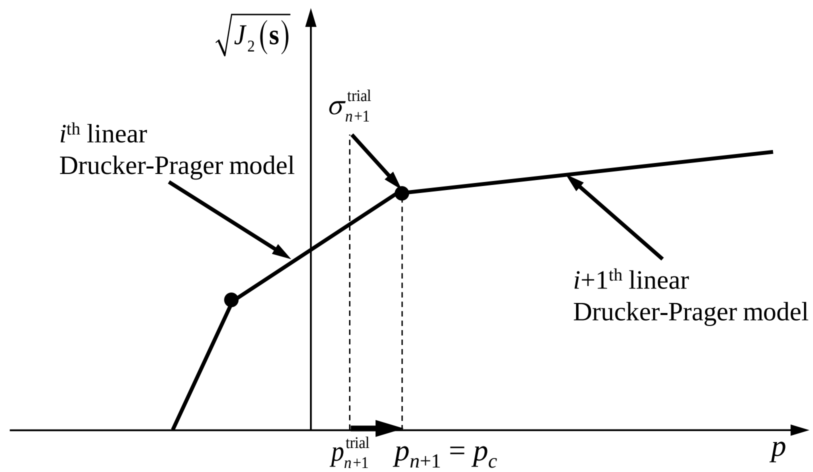

(b)

Fig. 4 Piecewise Drucker-Prager model; (a) inappropriate return mapping, (b) appropriate return mapping

2.2.4 Selection of the appropriate return mapping

Three return mappings are required in the PDP model. The selection procedure is summarized as follows. First, the values of p_{n+1} and p_c should be compared. If $p_{n+1} \geq p_c$ and

$$\sqrt{J_2(\mathbf{s}_{n+1})} = \sqrt{J_2(\mathbf{s}_{n+1}^{\text{trial}})} - G\Delta\gamma \geq 0 \tag{34}$$

then return mapping to the piecewise smooth portion is applied. In the above requirements, if condition $p_{n+1} \geq p_c$ changes as $p_{n+1} < p_c$, then return mapping to the corner should be applied. Otherwise, the return mapping to the apex has to be applied.

2.3 Consistent tangent operator

The elastoplastic tangent operator of the linear DP model is used in the PDP model. The elastoplastic tangents associated with the linear DP model have three possible forms. On the piecewise smooth portion return, associated elastoplastic tangent consistent is (de Souza Neto *et al*., 2008)

$$\begin{aligned}\mathbf{D}^{ep} = {} & 2G\left(1-\frac{\Delta\gamma}{\sqrt{2}\left\|\boldsymbol{\varepsilon}^{e\ \mathrm{trial}}_{d\ n+1}\right\|}\right)\mathbf{I}_{\mathbf{d}} + 2G\left(\frac{\Delta\gamma}{\sqrt{2}\left\|\boldsymbol{\varepsilon}^{e\ \mathrm{trial}}_{d\ n+1}\right\|}-GA\right)\mathbf{D}\otimes\mathbf{D} \\ & -\sqrt{2}GAK\left(\eta_i\,\mathbf{D}\otimes\mathbf{I}+\bar{\eta}_i\,\mathbf{I}\otimes\mathbf{D}\right)+K\left(1-K\,\eta_i\,\bar{\eta}_i\right)\mathbf{I}\otimes\mathbf{I}\end{aligned} \qquad \left(i=1,2,\ldots,n\right) \tag{35}$$

where $\boldsymbol{\varepsilon}^{e}_{d}$ is the deviatoric component of elastic strain, **D** and A is defined by

$$\mathbf{D}=\frac{\boldsymbol{\varepsilon}^{e\ \mathrm{trial}}_{d\ n+1}}{\left\|\boldsymbol{\varepsilon}^{e\ \mathrm{trial}}_{d\ n+1}\right\|} \quad ; \quad A=\frac{1}{G+K\eta_i\bar{\eta}_i+\xi_i^{2}H_i} \tag{36}$$

At the apex, the associated elastoplastic tangent consistent is

$$\mathbf{D}^{ep}=K\left(1-\frac{K}{K+\alpha_i\,\beta_i\,H_i}\right)\mathbf{I}\otimes\mathbf{I} \qquad \left(i=1,2,\ldots,n\right) \tag{37}$$

At the corner, due to the complexity of the formulas in the subsequent derivations, we define several parameters as follows:

$$\begin{aligned}&\mathrm{const1}=G+K\,\eta^{i}\bar{\eta}^{i}+(\xi^{i})^{2}H\\&\mathrm{const2}=G+K\,\eta^{i}\bar{\eta}^{i+1}+\xi^{i}\xi^{i+1}H\\&\mathrm{const3}=G+K\,\eta^{i+1}\bar{\eta}^{i}+\xi^{i}\xi^{i+1}H\\&\mathrm{const4}=G+K\,\eta^{i+1}\bar{\eta}^{i+1}+(\xi^{i+1})^{2}H\end{aligned} \tag{38}$$

$$
\begin{aligned}
&\mathrm{Q} = \frac{1}{\left(\mathrm{const1}\cdot\mathrm{const4} - \mathrm{const2}\cdot\mathrm{const3}\right)}\\
&\mathrm{V} = 2K\eta^i\bar{\eta}^{2i+1}\left(\eta-1\right) + \xi^{2i}\bar{\eta}^i H\left(\xi-1\right)\left(\xi-\bar{\eta}\right)\\
&\mathrm{W} = G\eta^i\bar{\eta}^i\left(\eta-1\right)\left(1+\bar{\eta}\right) + K\eta^{2i}\bar{\eta}^{2i+1}\left(\eta^2-1\right) + \eta^i\bar{\eta}^i\xi^{2i}H\left(\eta\bar{\eta}+\eta\xi^2-\xi-\bar{\eta}\xi\right)\\
&\mathrm{X} = K\eta^i\bar{\eta}^i\left(1+\bar{\eta}\right)\left(\eta-1\right) + H\xi^{2i}\left(\xi-1\right)^2\\
&\mathrm{Y} = 2G\eta^i\left(\eta-1\right) + K\eta^{2i}\bar{\eta}^{i+1}\left(\eta^2-1\right) + H\eta^i\xi^{2i}\left[\eta\left(1+\xi^2\right)-2\xi\right]
\end{aligned}
\tag{39}
$$

where H is the hardening modulus. Then, the associated elastoplastic tangent consistent is

$$
\begin{aligned}
\mathbf{D}^{ep} = {} & 2G\left[1-\frac{\left(\Delta\gamma^i+\Delta\gamma^{i+1}\right)}{\sqrt{2}\left\|\boldsymbol{\varepsilon}^{e\ \mathrm{trial}}_{d\ n+1}\right\|}\right]\mathbf{I_d} + 2G\left[\frac{\left(\Delta\gamma^i+\Delta\gamma^{i+1}\right)}{\sqrt{2}\left\|\boldsymbol{\varepsilon}^{e\ \mathrm{trial}}_{d\ n+1}\right\|} - G\mathrm{Q}\mathrm{X}\right]\mathbf{D}\otimes\mathbf{D} \qquad \left(i=1,2,\ldots,n-1\right)\\
& -\sqrt{2}G\mathrm{Q}K\left(\mathrm{Y}\mathbf{D}\otimes\mathbf{I}+\mathrm{V}\mathbf{I}\otimes\mathbf{D}\right) + K\left(1-K\mathrm{W}\mathrm{Q}\right)\mathbf{I}\otimes\mathbf{I}
\end{aligned}
\tag{40}
$$

3. Constitutive programming

Abaqus (2013) provides a useful user subroutine interface called UMAT that allows one to define complex or novel constitutive models that are not available with the built-in Abaqus material models. UMATs are written as FORTRAN code and then linked and compiled by Abaqus during numerical simulations.

We develop the UMATs for linear, bilinear and piecewise DP model for implementing the plastic behavior of pressure dependent materials, and those are available in Mendeley Data's 'UMATs for linear, bilinear and piecewise Drucker-Prager models, Lee *et al*. (2018)'.

4. UMAT program verification

The UMAT for both linear and piecewise DP models are verified. The UMAT for the linear DP model is compared with the constitutive equations of several materials. The UMAT for PDP model is verified by comparing the FEA results with the extended DP criterion

4.1 FE model

A three-dimensional (3D) FE model with single 8-node elements is created for single element triaxial test simulation by using commercial software Abaqus 6.13 program (Abaqus, 2013). The boundary conditions about the *xy*-plane, *xz*-planes and *yz*-planes are applied on five surfaces to fix the element. Pressure is applied to the single extra surface of the *xy*-plane.

4.2 Linear Drucker-Prager model

A linear DP model subroutine of the HYPLAS program (de Souza Neto *et al*., 2008) is used to develop the UMAT for the linear DP model.

Various pressure-dependent material properties (Table 1) obtained from the literature and are used in the single element FE model. The zero-pressure yield (equals the cohesion of the material) σ_o is related to the uniaxial compression yield strengths σ_{yc}, if hardening is defined by the σ_{yc}, as

$$\sigma_o = \left(1 - \frac{1}{3}\tan\beta\right)\sigma_{yc} \tag{41}$$

where β is friction angle of the material. The numerical results are then compared with the constitutive equations of the linear DP model for various materials, as shown in Fig. 5. The result shows that after yielding begins, the von Mises stress σ_v from the UMAT models is identical to that of the linear DP models.

Table 1 Material properties of pressure dependent materials obtained from the literature

material	Young's modulus E (GPa)	Poisson's ratio ν	σ_{yc} (GPa)[a]	β (°)[a]
Starphire	72.1[b]	0.222[b]	2.00	49
Borofloat	62.2[b]	0.195[b]	1.75	52
$Zr_{65}Cu_{15}Al_{10}Ni_{10}$	83.0[c]	0.369[c]	1.80	14
$Mg_{58.5}Cu_{30.5}Y_{11}$	53.9[d]	0.318[d]	0.94	29

[a] Rodríguez *et al*, 2012; [b] Dannemann *et al*., 2012; [c] Plummer *et al*., 2011; [d] Zheng *et al*., 2006

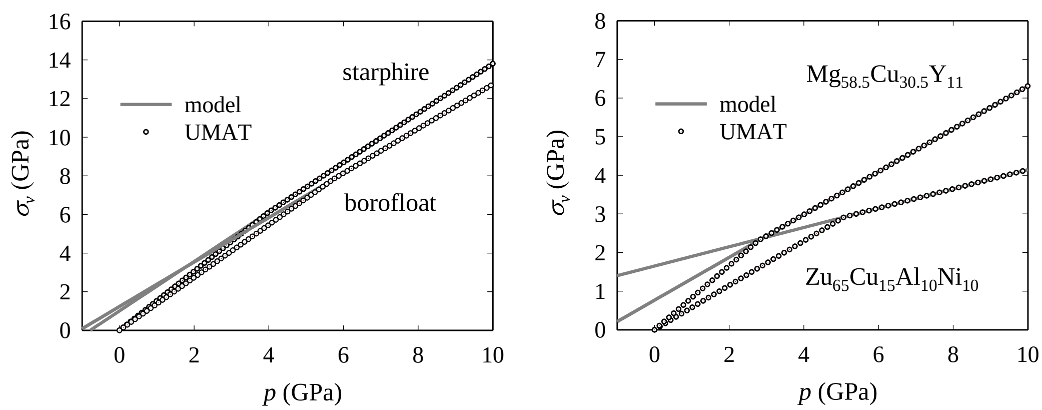

(a) **(b)**

Fig. 5 Comparison results of UMAT code with linear DP model for several materials; (a) ceramic glasses, (b) bulk metallic glasses

4.3 Piecewise Drucker-Prager model

The PDP model UMAT is developed to implement a pressure-dependent yield model that cannot be described by using existing DP models such as linear, hyperbolic, or exponent forms. The first example is for bilinear DP constitutive equation for failed borosilicate glass (Chocron *et al*., 2010). The constitutive equation is

$$\sigma = \begin{cases} 0.038+1.2p & p \le 1.72\ \text{GPa} \\ 2.1\ \text{GPa} & p > 1.72\ \text{GPa} \end{cases} \tag{42}$$

The Young's modulus E is $62.3\,\text{GPa}$, and the Poisson's ratio ν is 0.2. The comparison of results from the UMAT code with the DP constitutive equation for failed borosilicate glass is shown in Fig. 6a. The results show that after yielding begins, σ_v from UMAT model are identical to that of the bilinear DP model for failed boro-silicate glass.

The second example is for an extended Mohr-Coulomb model (Shafiq and Subhash, 2016), which is a generalized constitutive model for brittle ceramics that is expressed as

$$\tau = \tau_{\text{HEL}}\left(a + b e^{-k\left(\frac{P}{P_{\text{HEL}}}\right)}\right) \tag{43}$$

where τ is shear stress, τ_{HEL} is equivalent shear stress at the Hugoniot elastic limit (HEL) given by $\tau_{\text{HEL}} = \sigma_{\text{HEL}}/2$, a = 1.15, b = -1.06 and k = 1.78. Then multiplying both sides of Eq. (43) by 2, we obtain the extended Drucker-Prager (EDP) model, expressed as

$$\sigma_v = \sigma_{\text{HEL}}\left(a + b e^{-k\left(\frac{P}{P_{\text{HEL}}}\right)}\right) \tag{44}$$

The two pressure-dependent material properties obtained from the literature are listed in Table 2. The result of the UMAT code and the constitutive equation for EDP model is compared in Fig. 6b. The result shows that after yielding starts, the σ_v from the UMAT model are identical to that in the EDP model for SiC and soda-lime glass.

Table 2 Material properties of pressure-dependent materials obtained from the literature

material	E (GPa)	ν	σ_{HEL} (GPa)	P_{HEL} (GPa)
soda-lime glass	69.0[a]	0.23[a]	4.54[b]	2.92[b]
SiC	401.2[c]	0.186[c]	13[d]	5.9[d]

[a] Chen *et al*., 1995; [b] Holmquist *et al*., 1995; [c] Shackelford and Alexander; 2000, [d] Cronin *et al*., 2003

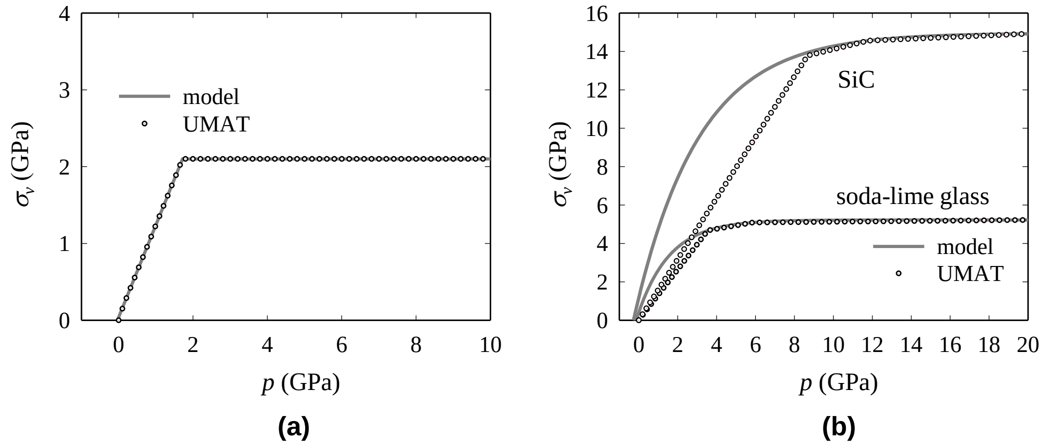

Fig. 6 Comparison results of UMAT code; (a) bilinear DP model for failed borosilicate glass, (b) EDP model for SiC and soda-lime glass

5. Summary

This study has derived constitutive equations for a piecewise Drucker-Prager (PDP) model and has developed integration algorithm based on the notion of return mapping to the smooth portion, apex, and corners. A consistent tangent operator with the developed integration algorithm was formulated for each return mapping case. The PDP model is then applied in commercial finite element code (using Abaqus) by developing a user material subroutine (UMAT). This UMAT for PDP model is verified through finite element analysis (FEA) of a hydrostatic test with a single element.

6. Acknowledgment

This research was supported by the Basic Science Research Program through the National Research Foundation of Korea (NRF-2017R1A2B3009706).

7. References

1. Abaqus User’s Manual, Version 6.13-2, Dassault Systémes Simulia Corp., Providence, RI.
2. Ansys 16.0 release documentation, “Theory and Modelling Guide,” ANSYS, Inc., Canonsburg, PA, 2015.
3. Chen, S.Y., Farris, T.N., and Chandrasekar, S., “Contact mechanics of Hertzian cone cracking,” International Journal of Solids and Structures, Vol. 32, pp. 329−340, 1995.

4. Chocron, S., Anderson JR, C.E., Nicholls, A.E., and Dannemann, K.A., “Characterization of confined intact and damaged borosilicate glass, Journal of the American Ceramic Society,” Vol. 93, pp. 3390−3398, 2010.
5. Cronin, D.S., Bui, K., Kaufmann, C., McIntosh, G., Berstad, T., and Cronin, D., “Implementation and validation of the Johnson-Holmquist ceramic material model in LS-DYNA.,” 4th European LS-DYNA Users Conference, pp. 47−60, 2003.
6. Dannemann, K.A., Anderson Jr, C.E., Chocron, S., and Spencer, J.F., “Damage development in confined borosilicate and soda-lime glass,” Journal of the American Ceramic Society, Vol. 95, pp. 721−729, 2012.
7. de Souza Neto, E.A., Peric, D., and Owen, D.R.J., “Computational methods for plasticity: theory and applications,” Wiley, 2008.
8. Drucker, D.C., and Prager, W., “Soil mechanics and plastic analysis or limit design, Quarterly of Applied Mathematics,” Vol. 10, pp. 157−165, 1952.
9. Holmquist, T.J., Johnson, G.R., Lopatin, C., Grady, D., and Hertel E.S. Jr, “High strain rate properties and constitutive modeling of glass,” 15th International Symposium on Ballistics, Jerusalem, 1995.
10. Lee, K., Marimuthu, K.P., and Lee, H., “UMATs for linear, bilinear and piecewise Drucker-Prager models,” Mendeley Data, v5, http://dx.doi.org/10.17632/5ccwt5fv7y.5, 2018.
11. Ma, G.W., Hao, H., and Zhou, Y.X., “Modeling of wave propagation induced by underground explosion, Computers and Geotechnics,” Vol. 22, pp. 283−303, 1998.
12. Milani, G., and Lourenco, P.B., “Blast analysis of enclosure masonry walls using homogenization approaches,” International Journal for Multiscale Computational Engineering, Vol. 7. pp. 91−113, 2009.
13. Plummer, J.D., Goodall, R., Figueroa, I.A., and Todd, I., “A study of mechanical homogeneity in as-cast bulk metallic glass by nanoindentation,” Journal of Non-Crystalline Solids, Vol. 357, pp. 814−819, 2011.
14. Rodríguez, M., Molina-Aldareguía, J.M., González, C., and LLorca, J., “Determination of the mechanical properties of amorphous materials through instrumented nanoindentation,” Acta Materialia, Vol. 60, pp. 3953−3964, 2012.
15. Shackelford, J.F., and Alexander, W., “CRC Materials Science and Engineering Handbook,” CRC Press, 2000.
16. Shafiq, M., and Subhash, G., “An extended Mohr-Coulomb model for fracture strength of intact brittle materials under ultrahigh pressures,” Journal of the American Ceramic Society, Vol. 99, pp. 627−630, 2016.
17. Zheng, Q., Ma, H., Ma, E., and Xu, J., “Mg-Cu-(Y, Nd) pseudo-ternary bulk metallic glasses: The effect of Nd on glass-forming ability and plasticity,” Scripta Materialia, Vol. 55, pp. 541−544, 2006.